The Astrophysical Journal, 798:92 (13pp), 2015 January 10 doi:10.1088/0004-637X/798/2/92

A STUDY OF VARIABILITY IN THE FREQUENCY DISTRIBUTIONS OF THE SUPERFLARES OF G-TYPE STARS OBSERVED BY THE *KEPLER* MISSION

Chi-Ju Wu[1], Wing-Huen Ip[1,2,3], and Li-Ching Huang[2]
[1] Graduate Institute of Space Science, National Central University, Taoyuan 32001, Taiwan; lu19900213@gmail.com
[2] Institute of Astronomy, National Central University, Taoyuan 32001, Taiwan
[3] Space Science Institute, Macau University of Science and Technology, Macau
Received 2014 April 29; accepted 2014 October 17; published 2014 December 31

ABSTRACT

The energy and time profiles of 4944 superflares from 77 G-type stars with well-defined light curve periodicities from the *Kepler* measurements have been analyzed in detail. The total value of the power-law index of the flare frequency distribution as a function of energy ($dN/dE \propto E^{-\gamma}$) between 5×10^{34} and 10^{36} erg is on average $\gamma = 2.04 \pm 0.17$, which is in agreement with previous results. The γ values of eight stars with frequent flaring activity vary between 1.59 ± 0.06 and 2.11 ± 0.19, suggesting a possible diversity of energy release effects. In general, stars with shorter rotation periods tend to have larger γ values. There is an indication that the flare energy is saturated at about 2×10^{37} erg. For a few large superflares of this energy range, it is found that their temporal behaviors could be characterized by a transition from single impulsive flares to long-duration flares composed of several flares.

Key words: stars: activity – stars: flare – stars: rotation – stars: solar-type – stars: statistics

1. INTRODUCTION

Solar flares are sudden explosions on the solar surface accompanied by a large release of energy of the order of 10^{29}–10^{32} erg on timescales from a few minutes to an hour (Shibata & Yokoyama 2002; Benz 2008). Although the mechanism of flares is not fully understood, it is generally believed to be associated with magnetic reconnection in the lower corona region between field lines emerging from the solar interior to the atmosphere (Shibata & Magara 2011). The largest solar flare (class X28+) ever recorded occurred on 2003 November 4, releasing 10^{32}–10^{33} erg on a timescale of about 400 s (Zhou et al. 2011).

In a statistical study of the flare activity of several F–M-type stars, Schaefer et al. (2000) found evidence that those so-called superflares have energies of about 10^{33}–10^{37} erg. More recently, the long-term observations of the *Kepler Mission* (Koch et al. 2010) provided a wealth of high-precision lightcurves, allowing detailed study of the stellar flare phenomena for different types of stars (Walkowicz et al. 2011; Maehara et al. 2012). Here, we are particularly concerned with the first detection of powerful white-light flares generated by G-type stars with energies approximately equal to those investigated by Schaefer et al. (2000).

One important question is whether the origin and dynamical behavior of these superflares are similar to those of solar flares, albeit of a much higher level ofenergy. One way to answer this question is to examine the occurrence frequency distribution of the flares as a function of the flare energy, or the flare frequency distribution, based on *Kepler* data. Using the measurements of solar hard X-ray burstsobtained by the *Solar Maximum Mission* (SMM), the flare frequency distributionwas found to be a power law

$$\frac{dN}{dE} \propto E^{-\gamma} \quad (1)$$

with the index γ estimated to be 1.8 (Dennis 1985) and 1.59 (Crosby et al. 1993), respectively. A survey of the γ values obtained from hard X-ray observations and soft X-ray observations by Crosby et al. (1993) showed the existence of a range of γ varying between 1.44 and 2.0. Such a power-law relation has been interpreted in terms of a self-organized criticality suggesting that solar flares are produced by a nonlinear energy dissipation system (Lu & Hamilton 1991; Wang & Dai 2013; Aschwanden 2014). From a statistical study of 1547 white-light flares with energy between 10^{33} and 10^{36} erg detected for 279 G-type stars selected from the *Kepler* data set, Shibayama et al. (2013) found that $\gamma \sim 2.2$ for G-type stars and $\gamma \sim 2.0$ for slow rotators with a rotation period of $\geqslant$10 days. Their result indicates that the superflares of G-type stars detected by the *Kepler mission* could have an energy release mechanism similar to that of the Sun.

The next question is then whether or not all of the flaring stars have similar γ values. Alternatively, might there be variation according to the physical properties of the stars, such as age and rotation period? Since a number of stars observed by *Kepler* have frequently occurring superflares, it is possible to compute and compare their individual power-law indices. The results are presented here. Section 2 will describe the data analysis procedure. Section 3 presents our results. A summary and discussion are given in Section 4.

2. OBSERVATION AND DATA ANALYSIS

The *Kepler* spacecraft was launched by NASA in 2009 March to search for super-Earths by finding transit events from the recorded light curves of target stars in the Cygnus–Lyra region (Borucki et al. 2010). The spacecraft carried a telescope with a 95 cm aperture and 105 deg^2 field of view, and the CCDs of the telescope have spectral response from 423 to 897 nmin optical range (Koch et al. 2010). About 160,000 stars in the Cygnus constellation region were continuously observed and recorded for a period of four years. The time resolutions of the *Kepler Mission* are 29.4 minutes for long cadence (LC) and 1 minute for short cadence (SC). The light curves of all 160,000 stars were recorded with LC data; only 512 of these light curves were sampled with SC data to support asteroseimic characterization (Gilliland et al. 2010). The typical photometric precision is 0.1 mmag for a star of 12 mag. Hence, the *Kepler Mission* provided long-term and high-precision observations that allow us to carry out comprehensive research in stellar physics.

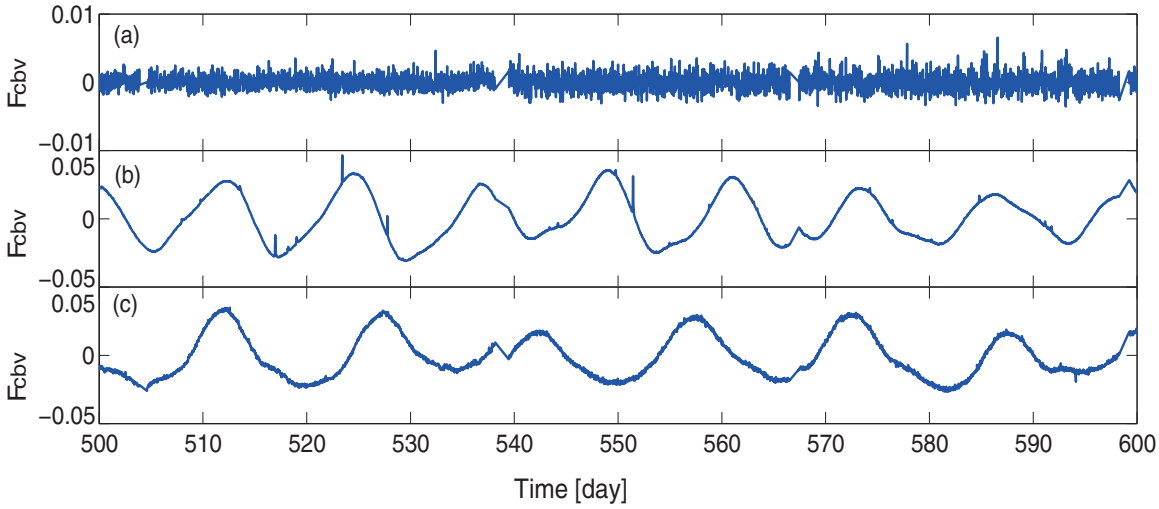

Figure 1. Comparison of the raw light curve (red) and the light curve after cotrending (blue) of KIC 893507 in Quarters 7 and 8. The median value of the cotrended light curve is indicated with the reddashed line in the middle panel. The final normalized light curve is obtained with formula (2), as shown in the lower panel.

From the early part (Q0–Q3) of the *Kepler* observations, Maehara et al. (2012) identified 146 flare stars out of a sample of 83,000 G-type stars. Based on this list, we choose 77 stars (Table 1) with well-defined periodicities in their light curves. Although such obvious light curve modulations can also be caused by binary systems or stellar pulsations, the possibility of pulsations is excluded because the timescale of G-type dwarf stellar pulsations is usually shorter than a half day. In addition, we examine the targets using an online binary catalog[4] which shows that none of the 77 stars in this work are eclipsing binaries. However, we cannot exclude the possibility that the stars are close binaries. Examining whether the flaring stars studied in this work are single or binary stars would require high-resolution spectroscopic measurements. We therefore assume that some of these stars are actually binaries and the flare mechanism might be associated with close binary RS CVn-type activity instead of the solar flare process, even though the periodic modulations in the light curves are presumed to be caused by star spots.

The data were retrieved from the Mikulski Archive at the Space Telescope Science Institute (MAST). Only the LC data, with >92% completeness (Kinemuchi et al. 2012), are used due to the requirement of continuous coverage without significant data gaps for light curve analysis.

The pipeline used in this paper is SAP_FLUX (labeled as raw data in fits files) from subtraction by the Cotrending Basis Vector (CBV) files fit with the PyKE[5] tool KEPCOTREND (Fröhlich et al. 2012; Still & Barclay 2012; Kinemuchi et al. 2012). CBV files are used to correct instrumental systematic trends in the *Kepler* light curves associated with spacecraft, detector, or environment effects rather than the target stars themselves. These CBV files are free to download at MAST.[6] We compare the differences between the cotrended light curves with the different numbers of basis vectors from the KEPCOTREND tool; for details on the use of this tool, refer to Barclay et al. (2012). We find that first using three to four vectors produces optimal results. The best number of CBVs to use for cotrending is target-dependent and purpose-dependent (Stark et al. 2013; Roettenbacher et al. 2013). Thus, to be on the safe side, we choose five basis vectors for cotrending all the light curves in this work. The time labels in this study are mission days, e.g., $t = \mathrm{BJD}-2454833.0$ (Gizis et al. 2013).

Figure 1 shows a comparison between the raw light curve, the cotrended light curves (CBVSAP_FLUX) obtained by subtracting the CBVs fit, and the normalized light curve of star KIC 893507 in Quarters 7 and 8. The systematic trend in the raw data (red curve in the upper panel) is eliminated through this procedure. The blue curve (F_{cbv}) in the middle panel shows the light curve after being cotrended using CBV files. The final light curve F_{norm} (in the bottom panel) has been normalized using the following formula where $\bar{F}$ is the median value of the flux:

$$F_{\mathrm{norm}} \frac{F_{\mathrm{cbv}} - \bar{F}}{\bar{F}}. \quad (2)$$

There are several ways to detect flares from light curves (Walkowicz et al. 2011; Osten 2012; Shibayama et al. 2013). One method is to subtract long-term stellar variability from the background and then select flare candidates from the detrended light curves. Figure 2 illustrates how the normalized flux curve (F_{norm}) in panel (a) can be further separated into the stellar background flux ($F_{\mathrm{background}}$) and the flare spikes. To obtain $F_{\mathrm{background}}$, we compute the four-point average and calculate the median absolute deviation (MAD) of the residuals. We scan across the light curve with MAD; if a data point is greater than six times the corresponding MAD, then it is seen as an outlier and is removed from the second-time four-point averaging. Using this method, we smooth the light curve, excluding outliers and possible flare candidates. The smoothed curve is shown in panel (b). The next step is to obtain the flare flux increase by subtracting F_{norm} from $F_{\mathrm{background}}$, or $F_{\mathrm{flare}} = F_{\mathrm{norm}} - F_{\mathrm{background}}$. The comparisons clearly show that this procedure allows the sharp peaks to show up more prominently and flares to be recognized more easily.

Following the above steps, an automatic flare detector is constructed to find flare candidates. First, a running difference is computed between the adjacent data points of a detrended light curve. Second, flare candidates are identified by searching for sudden brightness increases larger than three times the standard variation (σ). Note that the threshold value of 3σ is an empirical value; other values, such as 4.5σ, were also used (Walkowicz

[4] http://archive.stsci.edu/kepler/eclipsing_binaries.html
[5] http://keplergo.arc.nasa.gov/PyKE.shtml
[6] http://archive.stsci.edu/Kepler/cbv.html

Table 1
List of 77 G-type Stars Showing Superflares and Well-defined Periodic Light Curves

Kepler ID	$T_{\rm eff}$[a]	log g[b]	Mag[b]	$R_{\rm star}$[c] (in $R_\odot$)	$L_{\rm star}$[d] ($\times 10^{33}$ erg s^{-1})	$P_{\rm rot}$[e] (day)	N[f]	Flare Percentage[g] (%)	γ
893507	5421	3.97	12.51	1.68	8.55	10.93	61	7.72	1.38 ± 0.17
1995351	5746	4.73	12.97	0.66	1.68	3.19	37	4.85	1.65 ± 0.27
2158047	5374	4.30	13.97	0.71	1.46	5.40	51	5.11	2.06 ± 0.38
2303102	5350	4.21	12.96	1.25	4.52	20.87	7	0.73	1.22 ± 0.26
2304604	5593	4.47	14.90	0.77	2.03	1.69	36	3.35	1.58 ± 0.26
2439140	5763	4.68	11.92	0.82	2.64	8.77	12	1.11	1.73 ± 0.51
2696734	5372	4.52	14.67	0.82	1.97	8.39	8	1.02	0.92 ± 0.37
2712582	5429	3.98	13.99	1.76	9.44	8.33	18	1.80	1.86 ± 0.36
2849692	5661	4.60	15.50	0.79	2.25	5.49	25	3.97	1.81 ± 0.28
2860579	5403	4.52	14.24	0.76	1.72	5.06	63	6.71	1.31 ± 0.07
2862041	5713	4.38	13.50	1.00	3.75	5.35	24	2.30	0.76 ± 0.20
2987160	5603	4.37	14.56	0.84	2.45	2.93	105	11.29	1.69 ± 0.10
3118883	5413	4.45	14.35	0.82	2.05	8.54	56	6.39	1.50 ± 0.11
3425756	5712	4.56	15.35	0.73	1.98	1.71	90	8.60	1.43 ± 0.08
3557532	5499	4.61	14.35	0.66	1.42	2.04	196	17.95	2.11 ± 0.19
3869649	5513	4.45	14.28	0.90	2.61	1.90	50	5.68	1.76 ± 0.26
3939069	5143	4.51	14.02	0.77	1.46	19.54	12	1.49	1.49 ± 0.34
4449749	5406	4.56	14.68	0.75	1.68	5.74	55	4.96	2.08 ± 0.31
4543412	5489	4.24	11.16	0.87	2.43	2.16	48	4.99	1.38 ± 0.12
4742436	5979	4.15	10.60	1.28	7.38	2.32	57	5.94	1.28 ± 0.10
4749912	5755	4.25	14.07	1.12	4.86	5.14	72	7.10	1.59 ± 0.24
4831454	5534	4.59	10.69	0.74	1.80	5.18	16	1.83	1.23 ± 0.27
5179841	5402	4.20	13.08	1.38	5.73	5.03	28	2.59	1.54 ± 0.26
5427641	5353	4.36	14.53	0.85	2.07	3.41	38	4.20	0.99 ± 0.13
5445334	5349	4.68	12.79	0.70	1.40	4.96	14	1.80	1.15 ± 0.30
5528061	5600	4.56	14.90	0.81	2.29	3.79	85	6.85	1.53 ± 0.13
5529084	5565	4.58	15.47	0.74	1.87	9.85	42	4.68	1.87 ± 0.24
5616432	5973	4.35	13.82	1.02	4.69	4.53	44	4.77	1.53 ± 0.17
5896387	5774	4.36	13.23	1.02	4.04	3.78	72	7.58	1.98 ± 0.17
6032920	5916	4.59	13.49	0.79	2.67	3.18	58	5.80	1.67 ± 0.21
6034120	5624	4.65	14.88	0.78	2.13	5.82	128	13.43	1.55 ± 0.15
6691930	5584	4.48	15.50	0.82	2.28	13.32	89	8.65	1.43 ± 0.13
6697041	5514	4.41	14.35	0.65	1.38	15.68	80	9.65	1.15 ± 0.06
6865416	5466	4.43	13.70	0.82	2.13	3.28	147	11.93	1.77 ± 0.10
7174505	5444	4.41	14.54	0.81	2.05	3.75	122	12.34	1.64 ± 0.10
7256548	5543	4.92	15.48	0.70	1.62	6.30	25	2.54	0.91 ± 0.23
7264976	5402	4.05	11.97	1.59	7.56	12.63	47	4.44	1.12 ± 0.09
7287601	5718	4.56	14.59	0.77	2.24	15.71	21	2.68	1.65 ± 0.26
7532880	5820	4.41	13.05	0.96	3.76	2.13	159	15.24	1.90 ± 0.16
7902097	5831	4.62	12.26	0.86	3.04	3.50	95	10.22	1.51 ± 0.09
8009474	5544	4.59	15.34	0.74	1.85	15.29	31	2.92	0.93 ± 0.13
8074287	5741	4.43	14.27	0.92	3.27	2.88	160	14.43	1.87 ± 0.10
8076634	5453	4.74	15.16	0.78	1.89	5.97	45	4.06	1.52 ± 0.16
8143783	5918	4.59	15.71	0.76	2.51	0.74	66	10.51	2.45 ± 0.26
8302223	5949	4.53	14.40	0.85	3.16	9.62	18	1.54	0.85 ± 0.43
8359398	5340	4.71	14.08	0.69	1.36	13.02	17	1.47	1.10 ± 0.13
8479655	5414	4.60	12.76	0.64	1.22	9.52	61	7.29	1.03 ± 0.11
8482482	5741	4.50	15.31	0.85	2.78	4.59	57	5.06	1.72 ± 0.15
8491470	5526	4.89	14.32	0.78	1.98	4.33	56	5.06	1.37 ± 0.21
8604805	5587	4.48	14.60	0.77	2.02	2.83	95	8.22	1.92 ± 0.14
8613466	5817	4.53	14.77	0.84	2.84	2.41	93	8.15	1.66 ± 0.11
9149986	5541	4.35	14.26	0.80	2.11	1.42	75	7.27	1.35 ± 0.08
9150539	5712	4.50	15.15	0.74	2.04	3.25	109	9.15	2.29 ± 0.28
9459362	5663	4.59	14.09	0.68	1.67	12.43	73	8.03	1.66 ± 0.19
9583493	5739	4.53	12.66	0.76	2.21	5.31	16	1.73	1.10 ± 0.27
9652680	5841	4.80	11.21	0.83	2.83	1.40	63	6.66	0.65 ± 0.15
9653110	5474	4.40	12.85	0.74	1.75	3.13	158	16.95	1.64 ± 0.07
9764192	5760	4.64	12.94	0.88	2.97	3.50	50	4.49	1.31 ± 0.13
9764489	5640	4.73	14.13	0.81	2.36	10.74	30	3.61	1.52 ± 0.18
9897464	5797	4.42	15.01	0.93	3.47	3.34	72	5.93	1.78 ± 0.18
10287991	5599	4.75	15.95	0.70	1.70	0.91	27	2.99	1.67 ± 0.33
10422252	5266	4.22	13.63	0.84	1.89	5.26	177	15.74	1.75 ± 0.08
10453475	5473	4.47	14.19	0.76	1.81	15.17	24	3.37	1.17 ± 0.15
10489814	5755	4.72	14.69	0.67	1.72	3.17	46	3.76	1.38 ± 0.15
10528093	5405	4.52	13.56	0.74	1.65	12.24	32	3.07	1.49 ± 0.14

Table 1
(Continued)

Kepler ID	$T_{\rm eff}$[a]	log g[b]	Mag[b]	$R_{\rm star}$[c] (in $R_\odot$)	$L_{\rm star}$[d] ($\times 10^{33}$ erg s^{-1})	$P_{\rm rot}$[e] (day)	N[f]	Flare Percentage[g] (%)	γ
10646889	5701	4.44	13.59	0.89	2.95	5.53	42	4.07	1.44 ± 0.20
10745663	5990	4.59	14.34	0.95	4.12	3.14	137	12.53	1.63 ± 0.10
10796663	5502	4.16	13.15	1.33	5.71	7.18	25	2.85	1.21 ± 0.21
10969515	5420	4.49	14.42	0.79	1.91	5.30	44	4.04	1.67 ± 0.15
10992714	5659	4.30	14.99	1.08	4.17	2.22	55	4.72	1.30 ± 0.09
11235754	5458	4.56	15.22	0.78	1.90	6.71	37	3.34	1.16 ± 0.11
11235995	5379	4.52	15.04	0.83	2.05	5.14	120	8.55	2.07 ± 0.17
11551430	5541	3.72	10.69	1.60	8.48	4.14	202	18.56	1.59 ± 0.06
11764567	5480	4.38	13.22	0.78	1.94	19.42	59	7.70	1.39 ± 0.08
12003808	5401	4.76	15.90	0.60	1.09	3.63	73	5.97	1.70 ± 0.21
12266582	5689	4.34	12.95	0.92	3.15	6.82	12	1.47	1.53 ± 0.34
12401269	5748	4.42	14.29	0.88	3.01	2.23	94	10.62	1.61 ± 0.09

Notes.
[a] From the revised $T_{\rm eff}$ catalog (Pinsonneault et al. 2013).
[b] From the Kepler Input Catalog.
[c] From the revised stellar properties catalog (Huber et al. 2014).
[d] Stellar luminosity.
[e] Stellar rotation period by the Lomb–Scargle periodogram.
[f] Number of superflares.
[g] Flare occurrence frequency.

et al. 2011), and Shibayama et al. (2013) used three times the top 1% of the distribution. Third, to determine the end point of a flare, two criteria can be used according to the classical shape of a flare with exponential decay: (1) whether a data point in the decay phase is larger than the previous one; and (2) whether a data point in the decay phase is smaller than 5% of the peak flare amplitude.

Finally, the flare candidates could come from neighboring stars if the flare is strong enough to impact other pixels; also, the cosmic rays (CRs) can come from any angles. Although most of the CRs were identified and removed in the preliminary photometric analysis, some may remain unchecked. To eliminate the false candidates and CRs, the target pixel files (TPFs) are examined by eye to check the original pixel flare candidates' locations. If the pixels show flare-like events that do not correspond to the point-spread function of the target, then the candidates are removed.

In Figure 3, there are three flare candidates on KIC 2860579, KIC 10646889, and KIC 10745663, respectively. The left panels show the flare candidates with $F_{\rm flare}$. All three candidates display a good flare-like shape. The middle panels are bitmaps; no black or blue pixels are collected for the photometry stored in the light curve products. The white pixels are included in the photometric aperture that maximizes the target signal-to-noise ratio. For this bitmap, the white pixels are considered to be the PSFs of the targets in which the detected flares are very possibly generated by the target itself. The TPFs of these three candidates are presented in the right panels.

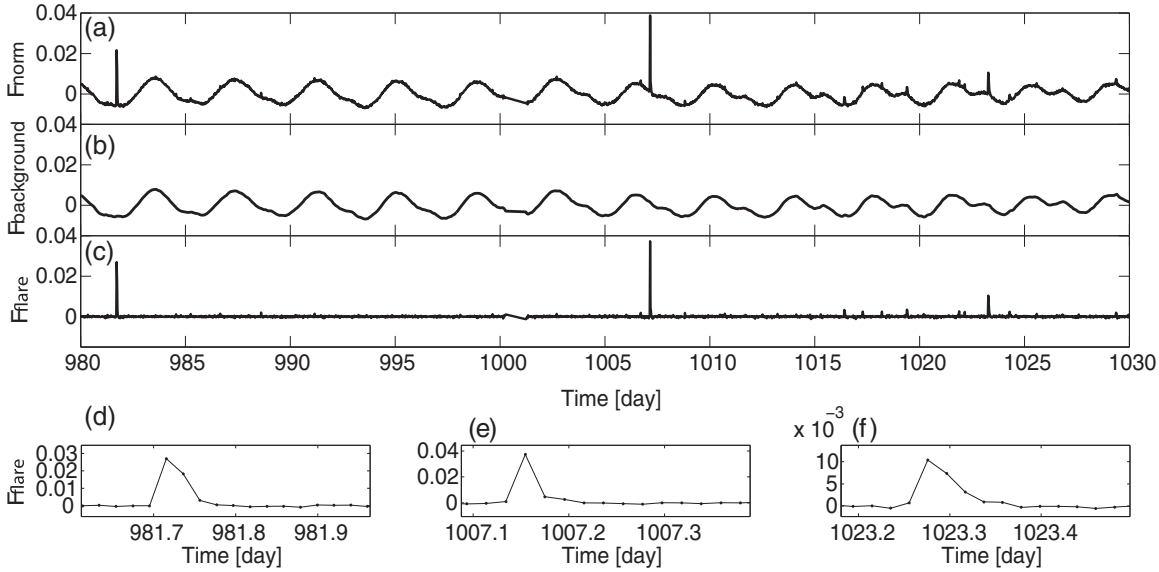

Figure 2. Panel (a) is the normalized light curve of KIC 5528061, which can be separated into background brightness variation (panel (b)) and the light curve only contributed by flare spikes (panel (c)). All of the upper panels (a) to (c) are shown in the same time interval (mission days 980–1030). The lower panels (d), (e), and (f) show three superflare examples after detrending.

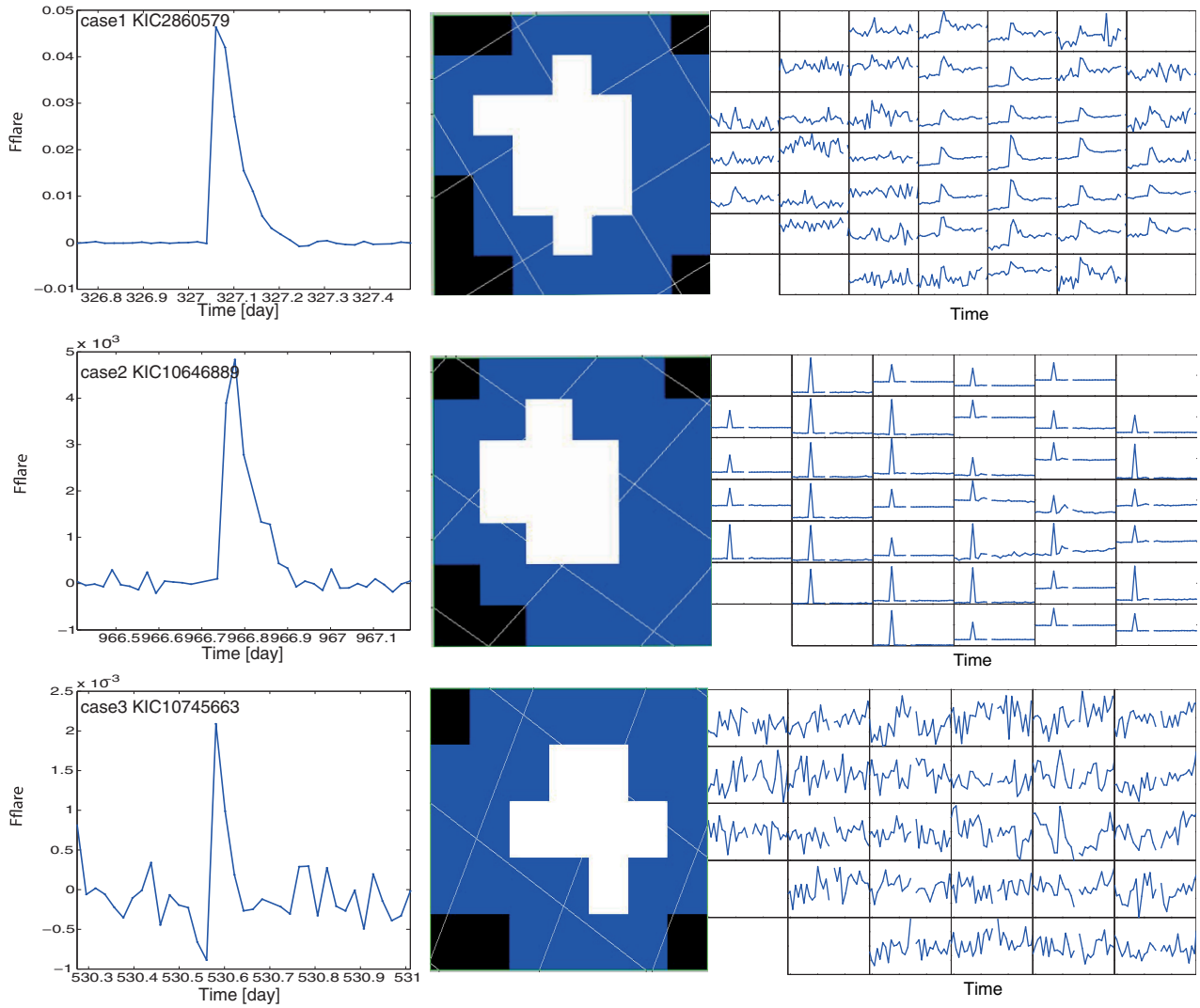

Figure 3. Time profiles of three flare candidates on KIC 2860579, KIC 10646889, and KIC 10745663, respectively. The timescales of these three cases are the same. Left panels show flare candidates with $F_{\rm flare}$, and the middle panels illustrate the bitmap of stars KIC 2860579, KIC 10646889, and KIC 10745663, with white pixels indicating the locations of targets. The right panels show the TPFs of three flare candidates. The first case (upper row) has a flux increase in the pixels corresponding to the target location. The second case (middle row) indicates a cosmic-ray hit. The third case has a flux fluctuation under the noise level.

For the first case on KIC 2860579, the pixels with flux increase events are matched to the PSF of the target (the upper row in Figure 3). However, in the second case, although the flare candidate on KIC 10646889 displays a good flare-like shape, it is a cosmic ray hit (middle row). Similarly, the candidate on KIC 10745663 has no obvious flux increase in TPF (lowest row); instead, the fluxes are all within the noise level. We check by eye using a strict standard, so even though the third case could be a small flare, it is removed. Among the 5584 superflare candidates, 11.5% have been found to be false events. In total, we have 4944 superflares on 77 G-type stars.

3. RESULTS

Since stellar flares are a kind of phenomena of energy release with sudden brightness increases, the corresponding flare energy can be estimated through the integration of the fluxes within the duration of the flares

$$E_{\rm flare} = \int L_* F_{\rm flare}(t)\ dt\ ({\rm erg}), \quad (3)$$

where $F_{\rm flare}$ is the normalized stellar flare flux, the peak value of which is the flare amplitude ($A_{\rm flare}$), as described in the previous section. The stellar luminosity L_* is calculated with the Stefan–Boltzmann law

$$L_* = 4\pi R_*^2 \sigma_{\rm sb} T^4\ ({\rm erg\ s^{-1}}), \quad (4)$$

where $\sigma_{\rm sb}$ is the Stefan–Boltzmann constant, R_* is stellar radius obtained from a catalog of revised stellar properties (Huber et al. 2014), and we use the effective temperature ($T_{\rm eff}$) from Pinsonneault et al. (2013).

The very large Halloween event, a class X17 solar flare, which occurred on 2003 October 28, had a peak amplitude of 0.027% and its energy was estimated to be roughly 6×10^{32} erg (Kopp et al. 2005). The superflares detected by *Kepler* (Maehara et al. 2012) have much larger energy ranging from 10^{33} to 10^{36} erg. The stellar flare peak amplitudes are correspondingly larger with $A_{\rm flare}$ between 0.03% and 15.8% of the stellar luminosity. In this work, the flare peak amplitudes have a minimum of about 0.01% and a maximum of 29.8%. Figure 4 shows a density map of the flare amplitude against the energy of the 4944 superflares selected in the previous section. It indicates that most of the flares have amplitudes between 0.2% and 2% of the stellar

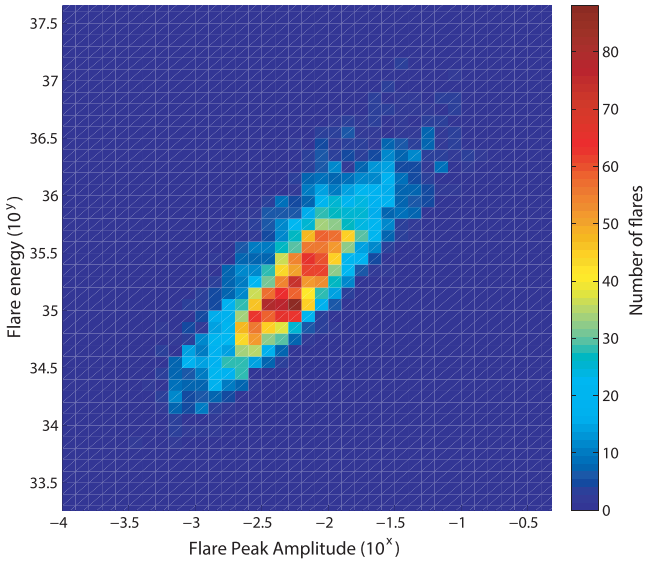

Figure 4. Correlation between flare energy (in erg) and peak amplitude normalized to stellar luminosity in the log scale. The color is the flare number in each pixel range.

luminosity and their energy ranges between 8×10^{34} and 3×10^{35} erg. There exists a clear linear dependence, or $E \propto A_{\rm flare}$.

Figure 5 depicts the variation of the flare energy as a function of the energy release time interval (flare duration). Because these samples were obtained in long cadence, the distribution is divided into discrete lines in 30 minute intervals and the shaded area is added to aid pattern recognition. The superflares usually last about several hours (<6 hr) according to the *Kepler* measurements. It is interesting to note that there seems to be an upper limit to the flare energy at about 2×10^{37} erg.

Several superflares with energy on the order of a few times 10^{36} erg are chosen from Figure 5, labeled with lowercase letters (a) to (p). Their time profiles are compared in Figure 6. All of the profiles are shown in the same time interval (0.5 days) and height (30%). As expected, for those flares with relatively short durations (~3–4 hr), the $A_{\rm flare}$ values are generally large and the decay phase tends to be smooth. On the other hand, for those with durations reaching four hours or more, the $A_{\rm flare}$ values are small while the time profile gives the impression of containing a number of bumps that could be generated by other flares created in nearly the same time frame. Because the $A_{\rm flare}$ values of long-duration flares are too small to see the flare profiles clearly, their profiles are enlarged in insets. More details of these superflares are listed in Table 2.

The flare frequency distribution of G-type stars has been investigated by Maehara et al. (2012) and Shibayama et al. (2013). In their studies, the collective values of the power-law index γ were estimated to be 2.2–2.3 by summing the superflares from a number of flaring stars. Here, we performed similar fitting to 4944 superflares on 77 G-type stars and found that $\gamma = 2.04 \pm 0.17$ (see Figure 7 (a)). This value may be considered as a benchmark since it is similar to the power-law index previously determined by Maehara et al. (2012). Will this relation hold for all flaring G-type stars? The *Kepler* observations provide us with a window to examine the flaring activities of G-type stars over a range of history. For example, young solar analogs with faster rotation might have more flares (Noyes 1985) and the energy release mechanisms could be somewhat different from those of older counterparts with slower rotation.

To explore this possibility, we have computed the power-law indices of eight G-type stars each with large numbers of flares. The total flare numbers of these stars are all more than 130 and the statistical results are therefore good enough. If the data of these eight stars are added together, the corresponding γ value is 1.81 ± 0.03 (see Figure 8(b)). Figure 8 shows the differential flare frequency distribution of those eight G-type stars. Their γ values vary from 1.59 ± 0.06 to 2.11 ± 0.19. This is in units of the number of flares per erg per year, computed by dividing the number of flares in individual energy bins by the total time of the *Kepler* data coverage. It is interesting to note that these frequently flaring stars all have short rotation periods of about two to four days. Their physical parameters are summarized in Table 3.

The relation between the stellar rotation period, temperature, flare percentage, and power-law index may help us to better understand stellar flares and stellar activity. Figure 9 presents a distribution of the γ values and the flare percentage of all 77 stars in a checkerboard pattern. The γ values cover a wide

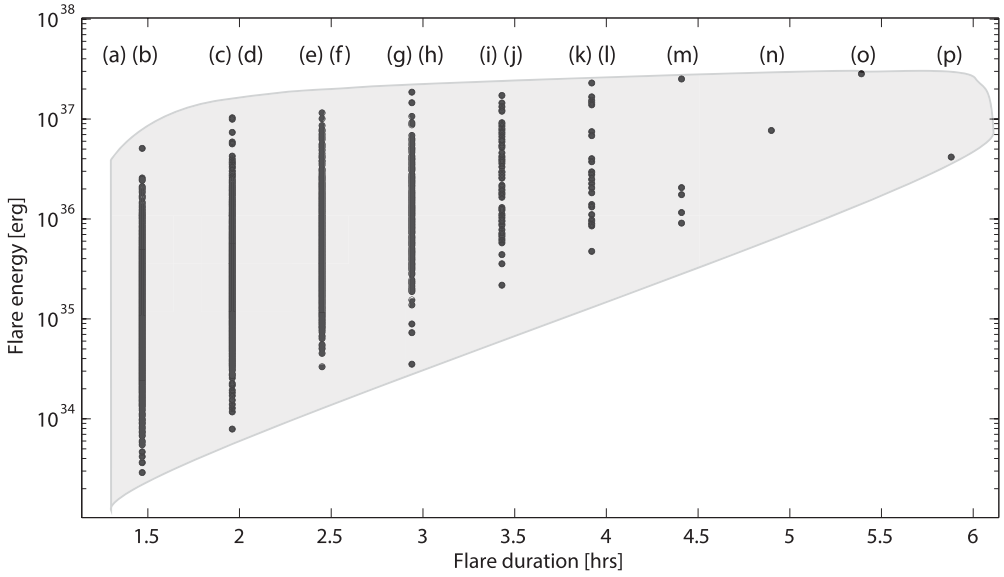

Figure 5. Distribution of the superflare energy as a function of energy release time. The shaded area is added to outline the pattern shown.

Table 2
Parameters of Superflares Present in Figure 6

Flare	Duration (hr)	Energy ($\times 10^{36}$ erg)	$A_{\rm flare}$ (%)	$A_{\rm spot}$ [a] (%)	Kepler ID[b]	$P_{\rm rot}$ [c] (days)	Flare Percentage[d] (%)
a	1.5	2.5	16.39	7.2	10287991	0.92	3
b	1.5	2.45	12.15	3.3	3869649	1.9	5.68
c	2	7.36	6.92	1.9	893507	10.93	7.73
d	2	5.74	29.8	10.7	10287991	0.92	2.99
e	2.5	11.54	27.43	5.1	10453475	15.17	3.38
f	2.5	7.09	9.96	9.58	12401269	2.23	10.63
g	3	18.61	5.77	2.1	11551430	4.15	18.56
h	3	14.57	5.88	2.7	11551430	4.15	18.56
i	3.5	13.26	3.27	3.6	893507	10.93	7.73
j	3.5	12	9.69	2.7	2860579	5.06	6.71
k	4	23	14.31	4.8	6691930	13.32	8.66
l	4	15.32	3.32	1.6	2860579	5.06	6.71
m	4.5	25.11	4.19	3.6	11551430	4.15	18.56
n	5	7.67	3.87	3.4	2860579	5.06	6.71
o	5.5	28.34	3.63	2.1	11551430	4.15	18.56
p	6	4.16	1.32	6.8	4543412	2.16	4.99

Notes.
[a] Amplitude of the star spot in $F_{\rm norm}$ at flare.
[b] Provided by the Kepler Input Catalog.
[c] Calculated by the Lomb–Scargle method.
[d] Percentage of total flare duration in the total observation period.

Table 3
Parameters of Stars Present in Figure 8

Kepler ID[a]	$P_{\rm rot}$ [b] (days)	N [c]	Flare Percentage[d] (%)	Largest Flare Energy ($\times 10^{36}$ erg)	Power-Law Index γ
11551430	4.15	202	18.5	28.34	1.53 ± 0.09
3557532	2.04	196	17.9	2.29	2.03 ± 0.16
10422252	5.26	177	15.7	2.32	1.91 ± 0.13
8074287	2.88	160	14.4	2.05	1.89 ± 0.11
7532880	2.13	159	15.2	6.87	1.98 ± 0.15
9653110	3.14	158	16.9	2.65.	1.85 ± 0.29
6865416	3.28	147	11.9	2.06	1.62 ± 0.15
10745663	3.14	137	12.5	2.38	1.42 ± 0.16

Notes.
[a] Provided by the Kepler Input Catalog.
[b] Calculated by the Lomb–Scargle method.
[c] Flare number in the observation period.
[d] Percentage of total flare duration in the total observation period.

range from 0.6 to 2.5. Concerning the 14 stars with a high flare percentage (>10%), it can be seen that the superflare power-law indices vary from 1.5 to 2.5.The flanking panels are the numbers of stars in each slice, with black lines representing the total population and the gray area representing frequently flaring stars. Generally, the indices of the 77 stars range from 1.1 to 2.2 and have large numbers between 1.5 and 1.7. In addition, as the flare number increases, the power-law indices tend to become more concentrated between 1.5 and 2.2.

Figure 10 shows the distribution of the power-law index γ as a function of the stellar rotation period and surface temperature. It can be seen that stars with higher surface temperature tend to rotate faster (Skumanich 1972; Palla & Stahler 1999; Kiraga & Stępień 2007), and the range of their individual power-law indices is more widespread and they tend to have larger values than those stars with slower rotation periods. Due to insufficient records of solar white-light flares, we use the empirical equation in Aschwanden (2014) to convert the power-law index in terms of the *GOES* 1–8 Å peak count rate (Dennis 1985) into bolometric energy in white-light. The resulting value is 2.19 ± 0.28, as indicated in Figure 10.

In this figure, we perform first-order fitting for these 77 stars with a red line. The black dashed line represents the median value of the 77 indices and the blue line represents the power-law index obtained from summing all of the superflares. The difference between the median value and the sum of all of the superflares is due to the fact that relatively more stars have flare energies in the range 10^{34}–3×10^{35} erg.

4. SUMMARY AND DISCUSSION

A flare is a phenomenon that releases a large amount of energy over a very short timescale. The details of flares and the relation between the flare mechanism and stars are still not well understood, yet it is believed that a flare is an energy burst of magnetic field structures in the stellar atmosphere via self-organized criticality. The power-law index γ in the energy–frequency distribution could be related to different

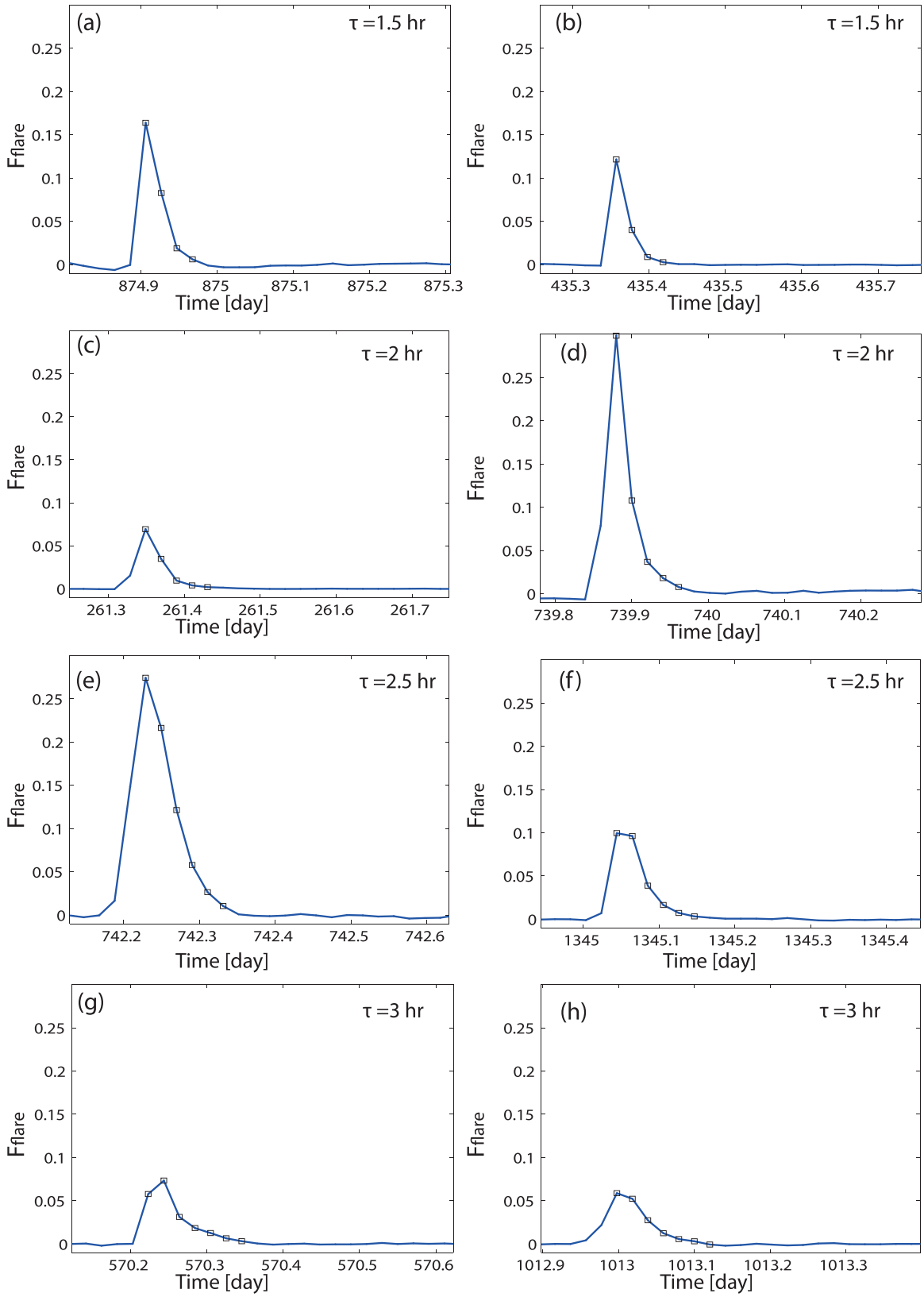

Figure 6. Time profiles of the 14 largest superflares chosen in Figure 5 shown in the same scale. The superflares are ordered by duration (τ). For those superflares with long durations and low amplitudes, the time profiles are detailed in the insets.

phases of stars. In this study, we introduce the methods for processing light curves, the criteria for selecting flares, and the definition of the flare end point. In total, 4944 superflares are selected from 77 G-type stars.

Earlier results (Maehara et al. 2012; Shibayama et al. 2013) showed γ values of ~2.2–2.3 from the statistical study of 365 and 1547 superflares, respectively. In this paper, we present the γ values of superflare frequency distributions, not only

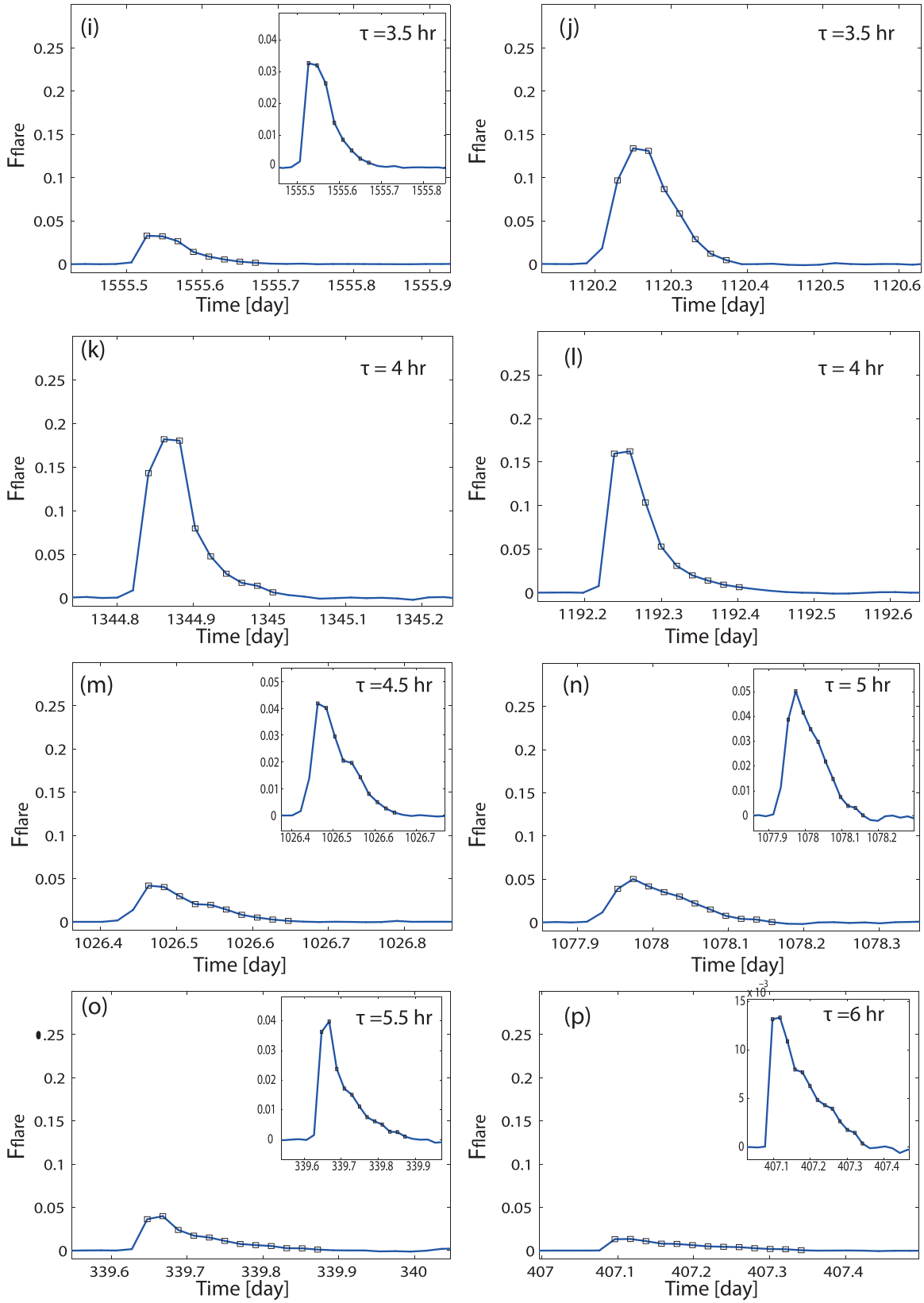

Figure 6. (Continued)

for all 4944 superflares on 77 G-type stars, but also for eight stars that have frequent superflares, providing enough data to obtain individual results. Our analysis shows that the total power-law index γ value for 4944 superflares is 2.04 $\pm$ 0.17, which corresponds well to previous estimates. Since this value is obtained from all of the superflares of 77G-type stars, the potential variation among different stars might be hidden from view. Therefore, we investigate eight stars selected for their

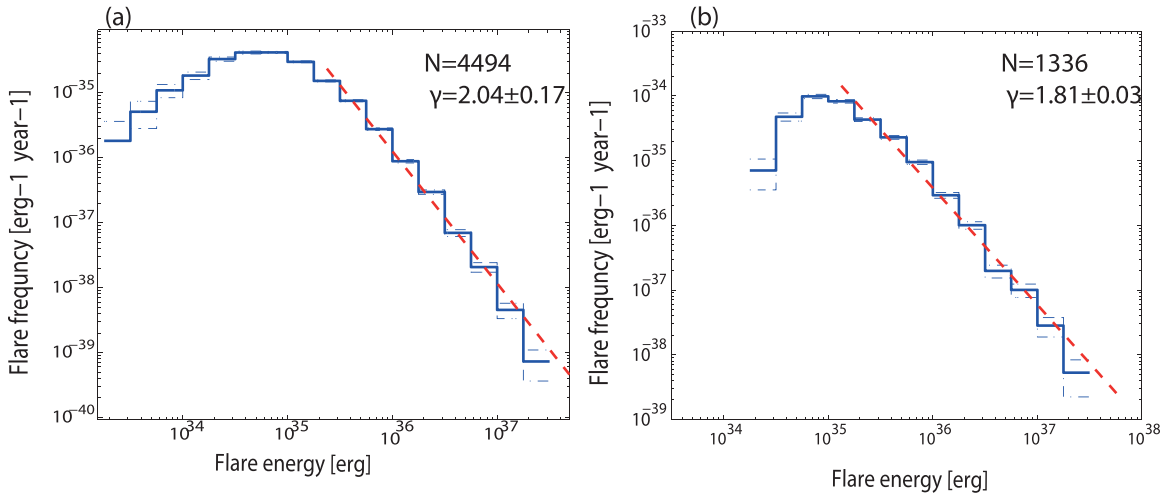

Figure 7. (a) Flare frequency distribution obtained from considering 4944 superflares on G-type stars, the power-law index γ of which is 2.04 ± 0.17. (b) The same as (a), but considering 1336 flares from eight stars with frequent flare activity. The power-law index γ is 1.81 ± 0.03. Error bars are estimated by the square root of numbers in each bin.

large number of flares; we find that the power-law indices γ values can vary significantly among individual stars, with their power-law indices varying from 1.59 ± 0.06 to 2.11 ± 0.19. For all 77 stars, the γ values vary from 0.65 ± 0.15 to 2.45 ± 0.26. Although the present work does not cover all of the flaring stars, our results demonstrate the variability in the power-law indices. Furthermore, despite power-law indices that vary significantly from star to star, there is a pattern that can be applied more widely and produce larger values for those stars with shorter rotation periods than for slowly rotating stars. Thus, there is a tendency for more active and fast rotating G-type stars to have larger γ values.

Another interesting phenomenon is that the energy of superflares apparently has a saturation value of about 2×10^{37} erg, which suggests that the stars might have an upper limit for the release of energy via flares. In this work, a sample of superflares with large energy is investigated in detail. It turns out that superflares with large energy and short duration tend to have higher amplitude and a smooth decay phase without bumps, which can be considered as a single, large stellar flare. On the other hand, superflares with long duration have smaller amplitudes; their flux profiles can be characterized by the presence of small-amplitude variation with several bumps, which could be explained as many small flares being triggered after the first flare in a nearby active region.

While the *Kepler* measurements have provided us with an unprecedented opportunity to investigate the flare activities of solar-type stars and other kinds of stars, interpretations of our results are still constrained by the limited number of samples listed in Maehara et al. (2012) and the length of time covered (~4 yr), photometric accuracy, and time resolution of the observations.The question remains of whether the inclusion of flares of smaller energy ($<10^{34}$ erg) and a more complete statistical study covering a wider energy range would modify the power-law distributions to the extent that individual G-type flare stars could on average have γ values similar to that of the Sun.

To address this issue, we have performed Monte Carlo tests simulating the occurrence frequencies of stellar flares according to a power-law distribution, say, with $\alpha = 1.80$. Using synthetic light curves, we compared the resultant statistical data obtained by counting the events with flare energy between 10^{32} erg and 10^{37} erg, and those obtained by counting events with flare energy between 10^{35} erg and 10^{37} erg. It was found that the corresponding power-law indices are similar within the error bars, i.e., 1.80 ± 0.04 versus 1.81 ± 0.12. Similar results were obtained with different power-law indices, thus giving us some confidence that the power-law indices derived from the *Kepler* observations should be representative of real effects. In any event, more complete data coverage will be essential in confirming such variability in the power-law indices for stellar flares.

It would therefore be most desirable to extend the complete coverage of stellar flares to energies well below 3×10^{33} erg, and hence the flare amplitudes to below 0.03%. This improved photometric capability will allow a much better understanding of the flare frequency distributions and the corresponding power-law behaviors of individual stars. It will be a major contribution to the study of the Sun in time and very useful for the study of the occurrence and evolution of stellar spots with small surface areas. By the same token, a much shorter cadence than is normally adopted for the *Kepler* measurements of 30 minutes will lead to new insights concerning the mechanisms of impulsive and gradual flares, as discussed here. We therefore look forward to the PLATO (Planetary Transits and Oscillations of stars) mission of ESA with a wide field ofview (2232 $\deg^2$) and short time resolution (25 s), which is designed to search for exoplanets and stellar oscillations (Rauer et al. 2014).

Finally, we note that some of the flaring G-type stars investigated in this work could have secondary companions that might be responsible for the energy release mechanism, as in the case of the RS CVns. High-resolution spectroscopic measurements such as those carried out by Wichmann et al. (2014) would be necessary to comprehend the physical properties of these *Kepler* super-flare stars. Some of the super-flaring stars studied by these authors turned out to be fast-rotating stars younger than the Hyades, some of which are binary in nature. We plan to pursue this line of investigations in future study.

We are thankful to the reviewer for useful comments and also to Professor Sami Solanki for comments and valuable suggestions. We also thank the Mikulski Archive at Space Telescope Science Institute (MAST) for providing free data access. This work is supported by NSC 101-2119-M-008-007-MY3 within the framework of the TANGO project and project

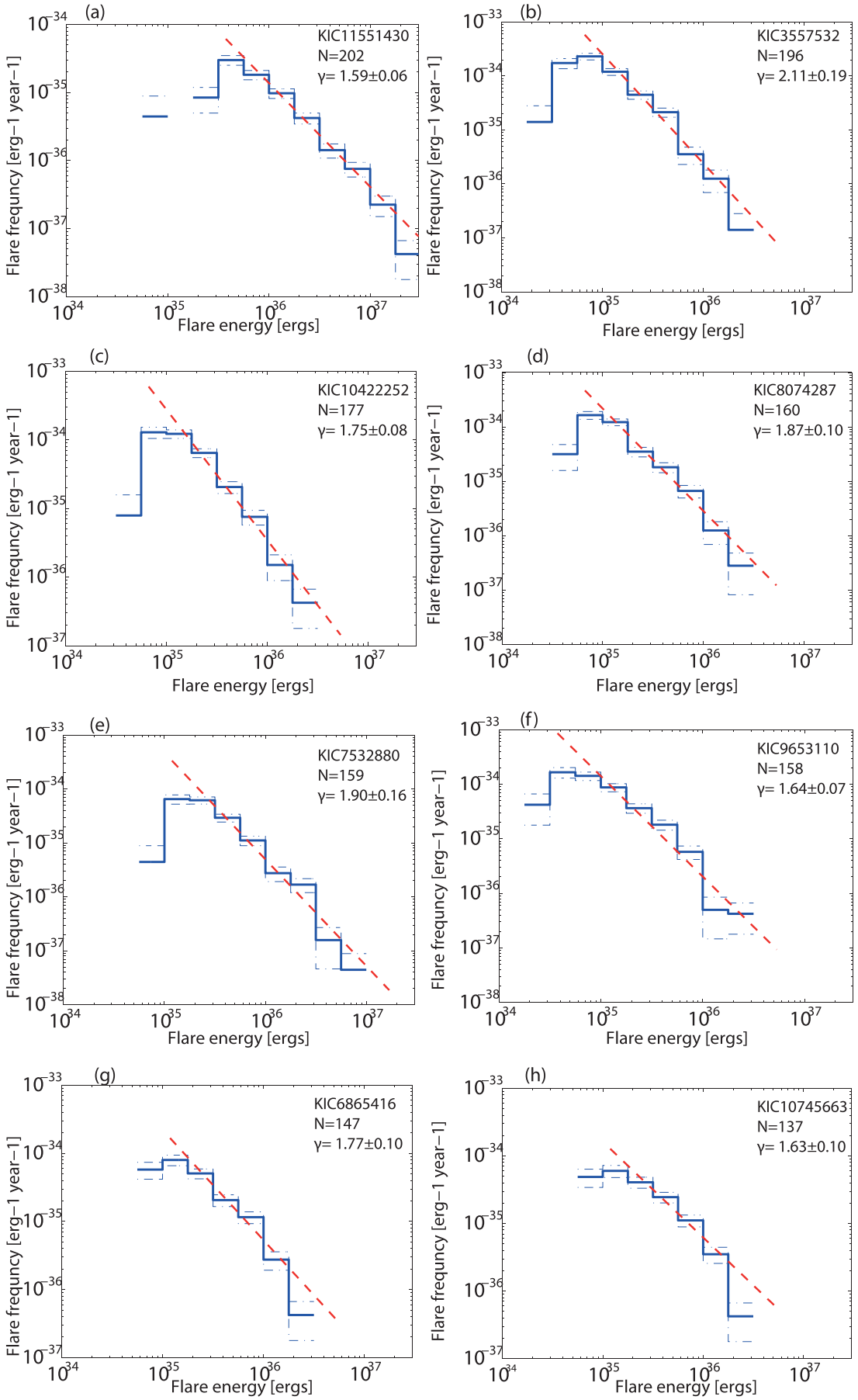

Figure 8. Flare energy frequency distributions of eight stars that have frequent flare activity. The unit of flare frequency is per erg per year. The error bars are estimated by the square root of the number in each bin width.

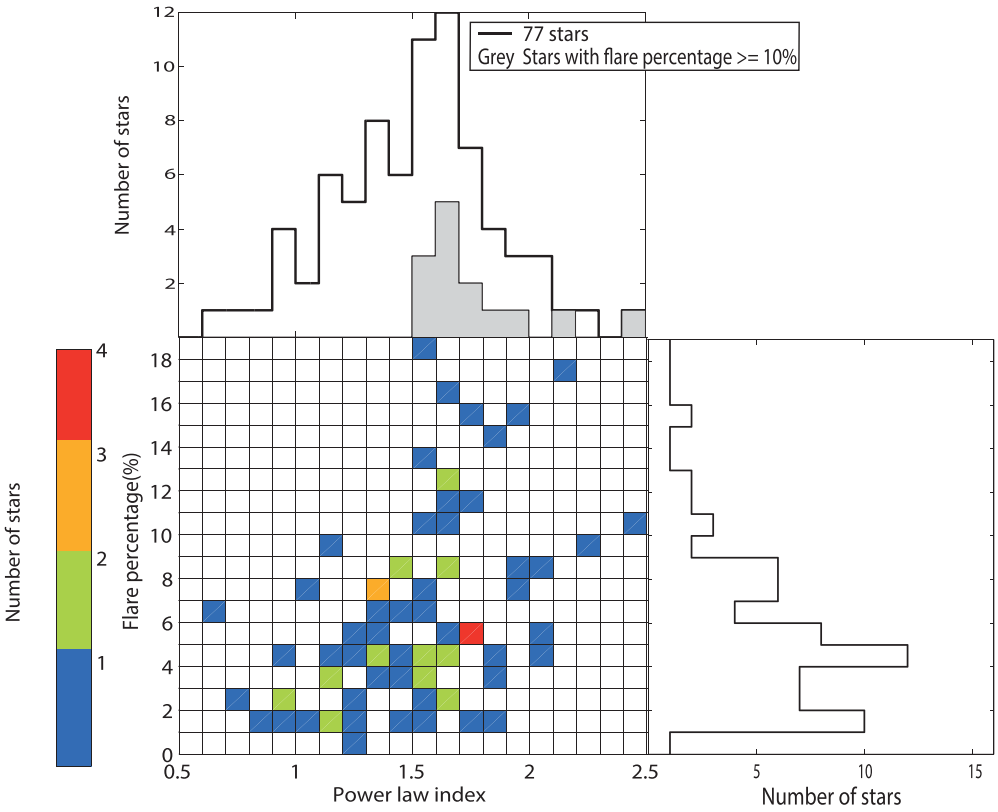

Figure 9. Checkerboard pattern depicting the distribution of the power-law indices of 77 G-type stars. The thick lines in the upper panel and the right panel show the total number of stars of each slice, and the thin line in the upper panel shows the number of stars with a flare percentage larger than 10%. Color represents the number of stars in each pixel.

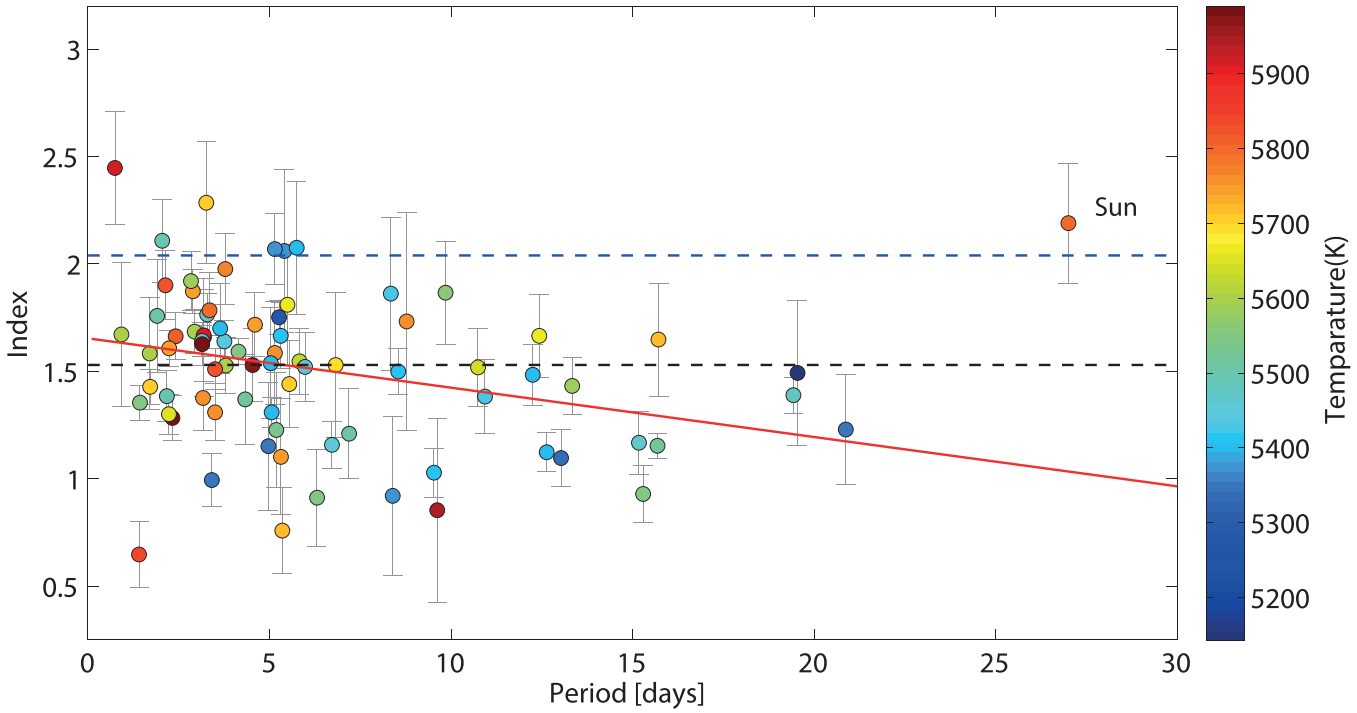

Figure 10. Scatter plot of power-law indices as a function of stellar rotation period. Color represents temperature. The temperature is obtained from the revised *Kepler* target property catalog. The red line presents the linear fitting of 77 stars (the Sun excluded). The black dashed line and blue dashed line represent the median of gamma values and the index value by summing all superflares, respectively.

019/2010/A2 of the Science and Technology Development Fund MSAR No. 0166.

REFERENCES

Aschwanden, M. J. 2014, ApJ, 782, 54
Barclay, T., Still, M., Jenkins, J. M., et al. 2012, MNRAS, 422, 1219
Benz, A. O. 2008, LRSP, 5, 1
Borucki, W. J., Koch, D., Basri, G., et al. 2010, Sci, 323, 977
Crosby, N. B., Aschwanden, M. J., & Dennis, B. R. 1993, SoPh, 143, 275
Dennis, B. R. 1985, SoPh, 100, 465
Fröhlich, H.-E., Frasca, A., Catanzaro, G., et al. 2012, A&A, 543, A146
Gilliland, R. L., Jenkins, J. M., Borucki, W. J., et al. 2010, ApJL, 713, L160
Gizis, J. E., Burgasser, A. J., Berger, E., et al. 2013, ApJ, 799, 172
Huber, D., Aguirre, V. S., Matthews, J. M., et al. 2014, ApJS, 211, 2
Kinemuchi, K., Barclay, T., Fanelli, M., et al. 2012, PASP, 124, 963
Kiraga, M., & Stępień, K. 2007, AcA, 57, 149
Koch, D. G., Borucki, W. J., Basri, G., et al. 2010, ApJ, 713, 79
Kopp, G., Lawrence, G., & Rottman, G. 2005, SoPh, 230, 129
Lu, E. T., & Hamilton, R. J. 1991, ApJ, 380, 89
Maehara, H., Shibayama, T., Notsu, S., et al. 2012, Natur, 485, 478
Noyes, R. W. 1985, SoPh, 100, 385
Osten, R. A. 2012, AUS, 285, 137
Palla, F., & Stahler, S. W. 1999, ApJ, 525, 772
Pinsonneault, M. H., An, D., Molenda-Żakowicz, J., et al. 2013, ApJS, 199, 30
Rauer, H., Catala, C., Aerts, C., et al. 2014, in Experimental Astronomy (Dordrecht: Springer), 41
Roettenbacher, R. M., Monnier, J. D., Harmon, R. O., et al. 2013, ApJ, 767, 60
Schaefer, B. E., King, J. R., & Deliyannis, C. P. 2000, ApJ, 529, 1026
Shibata, K., & Magara, T. 2011, LRSP, 8, 6
Shibata, K., & Yokoyama, T. 2002, ApJ, 577, 422
Shibayama, T., Maehara, H., Notsu, S., et al. 2013, ApJS, 209, 5
Skumanich, A. 1972, ApJ, 171, 565
Stark, C. C., Boss, A. P., Weinberger, A. J., et al. 2013, ApJ, 764, 195
Still, M., & Barclay, T. 2012, Astrophysics Source Code Library, 8004
Walkowicz, L. M., Basri, G., Batalha, N., et al. 2011, AJ, 141, 50
Wang, F. Y., & Dai, Z. G. 2013, NatPh, 9, 465
Wichmann, R., Fuhrmeister, G., Wolter, U., et al. 2014, A&A, 567, A36
Zhou, A. H., Li, J. P., & Wang, X. D. 2011, ApJ, 727, 42